Large dampinglike torque contribution originating from the orbital Rashba-Edelstein effect at a Pt/CoO interface

Bo Wang,[1] Yonghai Guo,[1] Xingrong Qi,[1] Bo Zhang,[1] Zhide Li,[2] Ziyang Hu,[2] Qi Wang,[3] and Jiangwei Cao[1,*]

[1]*Key Laboratory for Magnetism and Magnetic Materials of the Ministry of Education, Lanzhou University, Lanzhou 730000, People's Republic of China*

[2]*Shenzhen Yezhan Electronics Co., Ltd., Shenzhen 518000, People's Republic of China*

[3]*Dongguan Institute of Optoelectronics, Peking University, Dongguan 523808, People's Republic of China*

(Received 26 February 2024; revised 1 August 2024; accepted 19 August 2024; published 3 September 2024)

Current-induced spin-orbit torque (SOT) provides an efficient strategy for electrical manipulation of magnetism in spintronic devices. However, despite more than one decade of research for current-induced torque optimization, the charge-to-spin conversion efficiency and the resistivity in the spin-current source materials do not satisfy the requirement for next-generation low-consumption devices. Authors of recent theoretical works have predicted that an oxide or nitride interface can induce orbital angular momentum (OAM) accumulation through the orbital Rashba-Edelstein effect (OREE) and exert orbital torques to the adjacent magnetic layer. Here, we report on the remarkable dampinglike torque contribution from the OREE at the Pt/Co-O interface. In the Co/Co-O/Pt structures, the insertion of a thin natural-oxidized Co-O layer results in the sign reversal of SOT efficiency, suggesting the existence of a competing SOT source. In addition, the SOT efficiency and spin Hall magnetoresistance ratio in the Pt/Co structure were elevated significantly by introducing a Co-O underlayer. Anomalous SOT has also been observed in the Pt/Co/Co-O/Pt structures with perpendicular magnetic anisotropy by using the loop-shift technique and current-induced magnetization switching. After excluding the bulk contribution from the Co-O layer and its possible manipulation to the spin current from the Pt layer, we attribute this anomalous SOT origin to the OREE at the Co-O/Pt interface. In this paper, we not only provide a strategy for generating additional spin current for manipulating the SOT but also demonstrate an important clue toward microscopic understanding of how the out-of-equilibrium OAM interacts with the local magnetization.

DOI: 10.1103/PhysRevB.110.104404

In recent years, current-induced spin-orbit torque (SOT) and its driven magnetization switching in magnetic heterostructures have drawn much attention from the academic and industrial communities [1–5]. The SOT efficiency, which is crucial to realistic spintronic device application, depends on the charge-to-spin conversion rate in spin-current source layers and the transport and absorption of the spin current in the heterostructures [6–8]. The typical mechanism for charge-to-spin conversion includes the spin Hall effect (SHE) [9–11] in heavy metal (HM) and/or the Rashba-Edelstein effect (REE) [12,13] at their interface. Among all HMs, Pt has been the most widely investigated metal due to its large spin Hall angle and low resistivity [14,15]. In addition, extensive efforts have also been put forward to improve the SOT efficiency in the Pt-based system [16], for example, by introducing strong impurity scattering via MgO molecular doping [17] or introducing strong interfacial electron scattering via the insertion of submonolayers of Hf into Pt [17] and alloying Pt with Au [18] or Pd [19]. These approaches provide an alternative strategy with the potential to amplify SOT.

On the other hand, theoretical works have predicted an approach to the manipulation of magnetization based on electrically induced orbital current or orbital angular momentum (OAM) accumulation in nonmagnetic/ferromagnetic (FM) structures, known as the orbital Hall effect (OHE) [20–24] and orbital REE (OREE) [25–29]. Remarkably, both the OHE and OREE do not resort to spin-orbit coupling (SOC); they have been expected to appear in diverse material systems, for example, transition metals [21,22], two-dimensional materials [30,31], and Cu oxides or their interfaces [28,29,32–34]. Recent experiment works have demonstrated the large orbital torques [29,33–36], orbital Rashba-Edelstein magnetoresistance (MR) [34,37], and unidirectional orbital MR [38] in CuO/FM systems. Specifically, the significant enhancement of the SOT efficiency and spin-Hall MR (SMR) in thulium iron garnet (TmIG)/Pt by capping with a CuO_x layer suggests the orbital current generation at the Pt/CuO_x interface [29]. These results imply the important role of the oxides in the orbital-related effect. Beyond this, it was also found that the insertion of a naturally oxidized Co-O layer in the Pt/Co system may produce a sizable anomalous SOT [39–42]. Although the experimental result suggests the Co-O/Pt interface is important for this anomalous SOT, the specific physical mechanism has not been clarified clearly.

In this paper, we report on the manipulation of SOT and SMR by inserting a naturally oxidized Co-O layer in Pt/Co heterostructures. In the Co/Co-O/Pt structures, the SOT efficiency changes its sign with the increasing Co layer thickness, suggesting the existence of a competing SOT source in the

*Contact author: caojw@lzu.edu.cnx

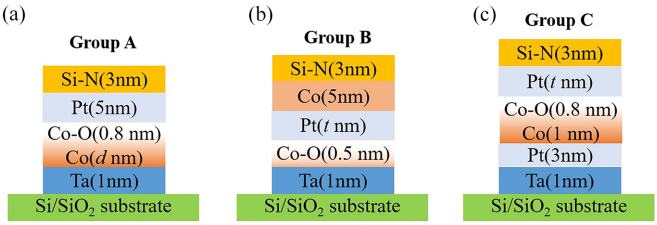

FIG. 1. The layer structures for three groups of samples: (a) Group A: Co/Co-O/Pt, (b) Group B: Co-O/Pt/Co, and (c) Group C: Pt/Co/Co-O/Pt.

structure. In contrast, in the Co-O/Pt/Co structure, we found a substantial increase in both the SOT efficiency and the SMR ratio in the thinner Pt regime. Anomalous SOT has also been observed in the Pt/Co/Co-O/Pt structures with perpendicular magnetic anisotropy (PMA) by using the loop-shift technique and the current-induced magnetization switching. In combination with the above results, we infer that the Co-O/Pt interface may contribute an additional SOT. Further, from the character of the FM thickness dependence of the measured SOT, we speculate that the anomalous extra SOT should originate from the OREE at the Co-O/Pt interface. In this paper, we highlight the importance of the orbital current effect in oxides structure and thus provide insights into engineering magnetic memory devices by simultaneously utilizing the spin and orbital current effect.

In this paper, three groups of samples shown in Fig. 1 were fabricated with the structure as follows: Ta(1)/Co(d_{Co})/Co-O(0.8)/Pt(5)/SiN(3) (group A), Ta(1)/Co-O(0.5)/Pt(t)/Co(5)/SiN(3) (group B), and Ta(1)Pt(3)/Co(1.0)/Co-O(0.8)/Pt(t)/SiN(3) (group C; the numbers in parentheses are layer thicknesses in nanometers). The film stacks were deposited on thermally oxidized Si substrates by magnetron sputtering with a base pressure prior to 2×10^{-7} Torr. In all the samples, 1-nm-thick Ta buffer layers and 3-nm-thick Si-N capping layers were deposited to form a good interface and prevent the possible oxidation of the films. In all samples, the Co-O layers were formed by natural oxidation of Co: After deposition of Co, the films were transformed to a load-lock chamber where they were exposed to the ambient atmosphere for an hour (the oxidization conditions are as follows: The pressure was ∼84.2 kPa, the temperature was ∼20 °C, and the relative humidity was ∼30–35%), resulting in the formation of a naturally oxidized Co-O layer. For comparative purposes, the films without the Co-O layer were also fabricated simultaneously. By investigating the Co layer thickness dependence of the magnetic moment per unit area in group A and comparing with the control samples (without natural oxidation), the oxidized Co layer thickness is determined to be ∼0.8 nm [43,44], and the saturation magnetization of the Co films is ∼ 1090 emu/cm^3 (see Supplemental Material S1 [45]). In the group B samples, 0.5-nm-thick Co layers were deposited and naturally oxidized in the air, ensuring the formation of a fully oxidized Co-O layer. The film stacks were subsequently patterned into Hall bar devices (200×10 um^2) for SOT measurement by standard photolithography and ion milling techniques.

We first measure the current-induced torques in group-A and B samples by utilizing the harmonic Hall voltage (HHV) technique [46,47]. In this measurement, an alternating current $I = I_0 \sin \omega t$ with the frequency of $f = \omega/2\pi = 133$ Hz was injected into the devices along the current channel (x axis). The current-induced alternating oscillation of magnetization produced a HHV via the anomalous Hall effect (AHE) and planar Hall effect (PHE). The time-dependent Hall voltage $V_H(t)$ was recorded by using a NI-PCI-4461 data acquisition card, then the first-HHV (V_H^{ω}) and the second-HHV ($V_H^{2\omega}$) were obtained by fast Fourier transformation of $V_H(t)$. The first and second harmonic Hall resistances were calculated by $R^{\omega} = V_H^{\omega}/I_0$ and $R_H^{2\omega} = I_0(\mathrm{d}R/\mathrm{d}I) = 2V_H^{2\omega}/I_0$, respectively. The azimuth angular (φ) dependence of R_H^{ω} and $R_H^{2\omega}$ were obtained by carrying out the above measurement in a rotating in-plane external magnetic field. The theoretical azimuth angular dependences of R_H^{ω} and $R_H^2\omega$ are expressed as follows [47]:

$$R_H^{\omega} = R_{\mathrm{AHE}} \cos\theta + R_{\mathrm{PHE}} \sin^2\theta \sin 2\varphi, \tag{1}$$

$$R_H^{2\omega} = \left[\frac{R_{\mathrm{AHE}} H_{\mathrm{DL}}}{2(H - H_{\mathrm{K}})} + R_{\Delta T}\right] \cos\varphi + \frac{R_{\mathrm{PHE}}(H_{\mathrm{FL}} + H_{\mathrm{Oe}})}{H} \cos\varphi \cos 2\varphi, \tag{2}$$

where R_{AHE}, R_{PHE}, and $R_{\Delta T}$ represent the anomalous Hall resistance, planar Hall resistance, and field-independent thermal Hall resistance associated with the anomalous Nernst effect (ANE) and spin Seebeck effect (SSE), respectively; H_{DL}, H_{FL}, H_{Oe}, and H_{K} represent the current-induced dampinglike (DL) effective field, fieldlike (FL) effective field, Oersted field, and the effective anisotropy field, respectively. Experimentally, R_{PHE} values are determined from the $R_H^{\omega}(\varphi)$ curve, while R_{AHE} and H_{K} values were estimated from the R_H^{ω}-H_Z curves.

Figure 2 shows the HHV measurement results for the group A samples. In these samples, the as-deposited Co layer thickness varies from 1.5 to 8 nm. After natural oxidation, 0.8-nm-thick Co layers were oxidized, and therefore, the residual Co layer thicknesses were in the range of 0.7–7.2 nm. Here, the marked thickness for the Co and Co-O layers are the residual Co thickness after natural oxidation and the oxidized Co layer thickness. The typical $R_H^{2\omega}(\varphi)$ curves measured under different field for the Co(1.7)/Co-O/Pt(5) and Co(4.2)/Co-O/Pt(5) samples are shown in Figs. 2(a) and 2(b), respectively. It is noted that the $R_H^{2\omega}(\varphi)$ curves are dominated by the $\cos\varphi$ term for both samples, but the field dependences are totally different for the two samples. For the Co(1.7)/Co-O/Pt(5) sample, the magnitude of the $\cos\varphi$ term decreases with increasing magnetic field, while an opposite variation trend was observed for the Co(4.2)/Co-O/Pt(5) sample. This different variation trend indicates the opposite sign of the DL torque in the samples with different d_{Co}. We then carried out the theoretical fitting to the experimental curves by using Eq. (2) and obtained the magnitude of different terms. Figure 2(c) plots the magnitude of the $\cos\varphi$ term as the function of $1/(H - H_{\mathrm{K}})$ for the samples with different d_{Co} and the linear fitting to them. According to Eq. (2), the slope of the linear fit to the $R_H^{2\omega,\cos\varphi}(\varphi) \sim 1/(H - H_{\mathrm{K}})$ curve is proportional to H_{DL}. From the linear fitting, we obtained H_{DL} values and then calculated the spin-torque efficiency per unit applied electric field by $\xi_{\mathrm{DL}}^{\mathrm{E}} = \frac{2e}{\hbar} \frac{M_{\mathrm{S}} d_{\mathrm{Co}} H_{\mathrm{DL}}}{E}$, with e, $\hbar$, and M_{S}

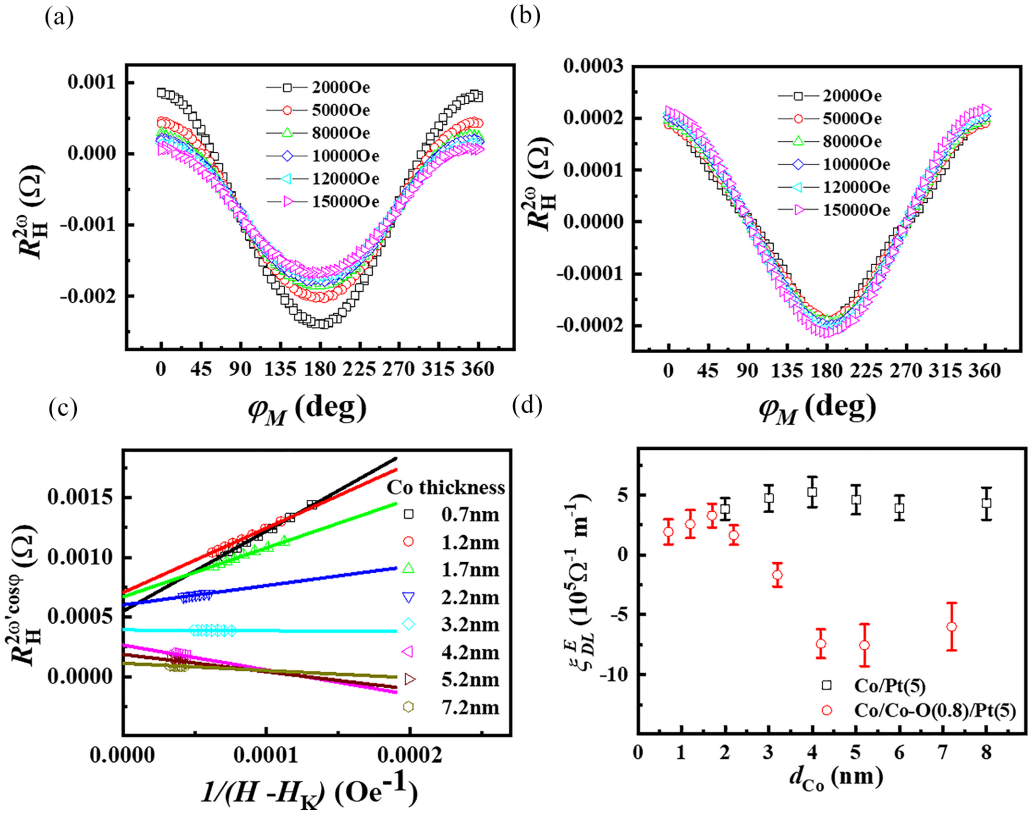

FIG. 2. The spin-orbit torque (SOT) measurement results for the Co/Co-O/Pt structures. The azimuth angular dependence of $R_H^{2\omega}$ under different external fields for the (a) Co(1.7)/Co-O/Pt(5) and (b) Co(4.2)/Co-O/Pt(5) samples. (c) The coefficients of cosφ term as the function of $1/(H - H_K)$ for the samples with different d_{Co}. (d) SOT efficiency variation for the Co(d_{Co})/Co-O/Pt samples and its comparison with the Co/Pt control samples.

being the elementary charge, the reduced Planck constant, and the saturation magnetization of the Co layer. Figure 2(d) summarized the measured ξ_{DL}^E for all the samples. It is noted that ξ_{DL}^E increases slightly with d_{Co} as $d_{Co} < 1.7$ nm, then it decreases and changes the sign as d_{Co} increases further and finally reaches a negative saturation value.

Now we discuss the possible mechanism for this unusual Co thickness dependence of the measured SOT. The initial increase of ξ_{DL}^E with increasing d_{Co} in the $d_{Co} < 1.7$ nm range may be ascribed to the increasing absorption to the spin current from the Pt layer [48,49]. However, the subsequent decrease of ξ_{DL}^E and its sign change cannot be explained in the SHE scenario. In addition, we did not observe any significant variation of ξ_{DL}^E for the control samples (without the Co-O layer) with d_{Co} in the range of 2–8 nm. These results suggest that, for the measured SOT in the Co/Co-O/Pt samples, in addition to the contribution from the SHE in the Pt layer, there exists a competing torque origin that is Co thickness dependent. We speculate that the Co-O insert layer may manipulate the SOT by the following several ways: (a) the Co-O layer itself may act as a new SOT source; (b) the extra Co/Co-O and Co-O/Pt interfaces may produce spin accumulation by the Rashba-related effect and exert torques to the adjacent Co layer; and (c) Co-O itself and its interface do not contribute extra spin current source, but it may affect the transport of the spin current from the Pt layer [50,51]. To recognize the actual mechanism from the above-mentioned possibilities, we fabricated a control sample with the structure of Co(4.2)/Co-O(0.8)/Si-N(3), the HHV measurement indicates that almost no SOT is observed in this structure (see Supplemental Material S2 [45]). This excludes the possible SOT contribution from the Co-O layer and the Co/Co-O interface. In addition, we also noted that previous studies have shown that the insertion of an antiferromagnetic insulator (AFMI) between the HM and the FM layer may manipulate the SOT efficiency by tuning the interface spin mixing conductance. However, this effective SOT manipulation generally occurs near the Néel temperature of the AFMI [52]. In our Co/Co-O(0.8)/Pt samples, the Néel temperature of the 0.8-nm-thick Co-O layer is far below room temperature, i.e., it is paramagnetic at room temperature. Although it is reported that the magnon spin current can be produced and transmitted in a paramagnet, the transport efficiency decreases with increasing temperature [53,54], inconsistent with the observed temperature dependence of SOT efficiency in these samples (see Supplemental Material S3 [45] about the measured temperature dependence of SOT for a typical sample with Co-O inserting layer). Therefore, the major role of the interfacial oxidized layer is to suppress spin-current transport due to the insulating nature. Moreover, the manipulation of SOT by magnon spin current cannot explain the observed sign change of the SOT with the variation of d_{Co}. Therefore, the only possible origination of the extra SOT is the Co-O/Pt interface, and its strong FM layer thickness dependence hints that the torque is related

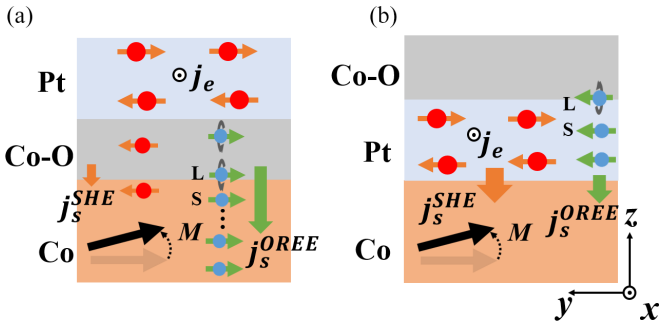

FIG. 3. Schematic illustration of nonlocal generation of the anomalous spin-orbit torque (SOT) in Co/Co-O/Pt and Co-O/Pt/Co structures via the orbital Rashba-Edelstein effect (OREE) at the Co-O/Pt interface. (a) The orbital angular momentum (OAM, indicated by green circulations) accumulation generated at the Co-O/Pt interface via OREE is converted to spin current (indicated by green arrows) by spin-orbit coupling (SOC) of Co, which exerts torques on the Co magnetization, as the spin-polarization direction from the OREE is opposite to the spin polarization (indicated by red arrows) from the spin Hall effect (SHE) in the Pt layer, resulting in the competing SOT in this system. (b) In Co-O/Pt/Co structures, the OAM from the Co-O/Pt interface is converted to spin current by SOC of Pt, which converges with the spin current from the SHE in the Pt layer and results in the enhanced SOT in the CoO/Pt/Co structures.

to the orbital-related effect. The OREE at the Co-O/Pt interface is the most plausible mechanism, in which the inversion symmetry is broken at the interface, and orbital asymmetry leads to the Rashba-type texture of the OAM. As shown in Fig. 3(a), the orbital accumulation at the Co-O/Pt interface diffuses into the FM layer and transforms into the spin current by SOC of Co. However, the orbital current diffusion length is much large than that of spin current [24,38,55]; therefore, the OREE-induced torque becomes significant and dominates in this structure only when the Co layer reaches a certain thickness. Assuming that the spin and OAM arriving at the Co layer has the opposite direction (see Supplemental Material S4 [45] about the discussion on the spin and the OAM direction in these structures), this explains the sign change of the measured SOT in the Co/Co-O/Pt structure. In addition, previous works have demonstrated that a HM layer with strong SOC can help to convert orbital current to spin current [29,36]. Therefore, the orbital current originated from the OREE at the Co-O/Pt interface may also diffuse into the Pt layer and convert to spin current efficiently due to the large SOC in the Pt layer. This additional spin current is combined with the spin current generated by the SHE in the Pt layer, resulting in an enhanced SOT on the adjacent Co layer, as shown in Fig. 3(b). Based on this discussion, we designed the group-B samples and measured the SOT and SMR by the harmonic technique.

Figure 4(a) shows the coefficients of the $\cos\varphi$ term in $R_H^{2\omega}/R_{\mathrm{AHE}}$ as the function of $1/(H-H_{\mathrm{K}})$ for the Co-O(0.5)/Pt(2.5)/Co(5) sample and the Pt(2.5)/Co(5) control sample at the same current density. As discussed previously, the slope of $R_H^{2\omega,\cos\varphi}/R_{\mathrm{AHE}} \sim 1/(H-H_{\mathrm{K}})$ curve in the HHV measurement corresponds to the DL-SOT effective field. Therefore, a significant DL-SOT enhancement is observed as a thin Co-O layer is inserted under the Pt layer. We systematically studied the evolution of $\xi_{\mathrm{DL}}^{\mathrm{E}}$ for the Co-O(0.5)/Pt(t_{Pt})/Co(5) samples and the Pt(t_{Pt})/Co(5) control samples with various t_{Pt}. As shown in Fig. 4(b), for the Pt(t_{Pt})/Co(5) control sample without a Co-O layer, the Pt thickness dependence of $\xi_{\mathrm{DL}}^{\mathrm{E}}$ can be fitted well by a simple spin-diffusion model of the SHE scenario $\zeta_{\mathrm{DL}}^{\mathrm{E}} = \frac{2e}{\hbar}\sigma_{\mathrm{SH}}[1-\mathrm{sech}(t_{\mathrm{Pt}}/\lambda_{\mathrm{sf}})]$, where σ_{SH} is the spin Hall conductivity, and λ_{sf} is the spin-diffusion length in the Pt. From the fitting, we obtain spin Hall conductivity $\sigma_{\mathrm{SH}} = (5.0 \pm 0.5) \times 10^5 (\hbar/2e)\,\Omega^{-1}\,\mathrm{m}^{-1}$ and spin diffusion length $\lambda_{\mathrm{sf}} = 2.2 \pm 0.3$ nm. The effective spin Hall angle can be estimated to be $\theta_{\mathrm{SH}} = (2e/\hbar)\sigma_{\mathrm{SH}}\rho_{\mathrm{Pt}} = 0.15 \pm 0.02$ with the Pt resistivity $\rho_{\mathrm{Pt}} = 3.0 \times 10^{-7}\,\Omega\,\mathrm{m}$. In contrast, the samples with Co-O underlayers exhibit a completely different dependence on t_{Pt}: Here, $\xi_{\mathrm{DL}}^{\mathrm{E}}$ first increases abruptly and reaches a maximum at $t_{\mathrm{Pt}} = 2.5$ nm, then it decreases and regains the same value at $t_{\mathrm{Pt}} > 6$ nm as the samples without a Co-O underlayer. It is noted that the maximum of $\xi_{\mathrm{DL}}^{\mathrm{E}}$ in the Co-O(0.5)/Pt(t_{Pt})/Co(5) sample is about twice of the measured σ_{SH} in the Pt/Co(5) samples, suggesting the significant enhancement of the DL-SOT by a thin Co-O underlayer.

To corroborate the extra spin-current origin in the Co-O(0.5)/Pt(t_{Pt})/Co(5) samples, we studied the effects of the Co-O underlayer on SMR. In the SMR scenario [56–58], the spin current reaching the HM/FM interface can be partially

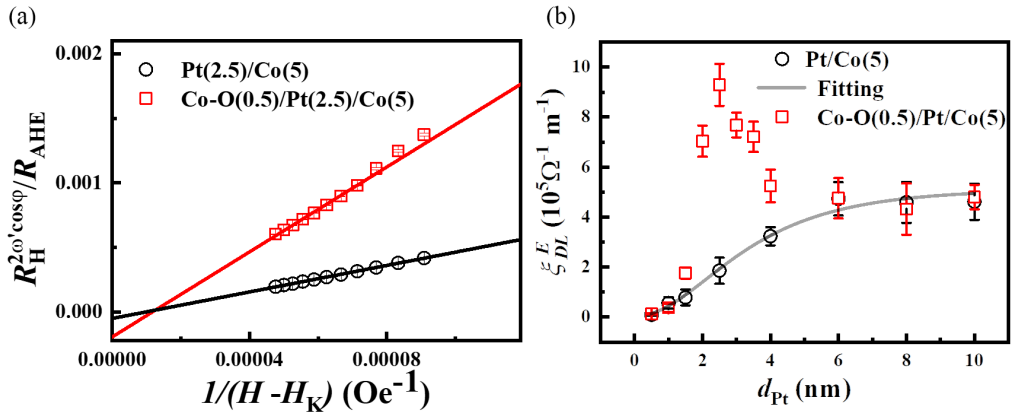

FIG. 4. The harmonic Hall voltage (HHV) measurement results for the Co-O/Co/Pt structures. (a) The coefficients of the cosφ term as a function of $1/(H-H_{\mathrm{K}})$. (b) The calculated dampinglike spin-orbit torque (DL-SOT) efficiency for the samples with different t_{Pt}.

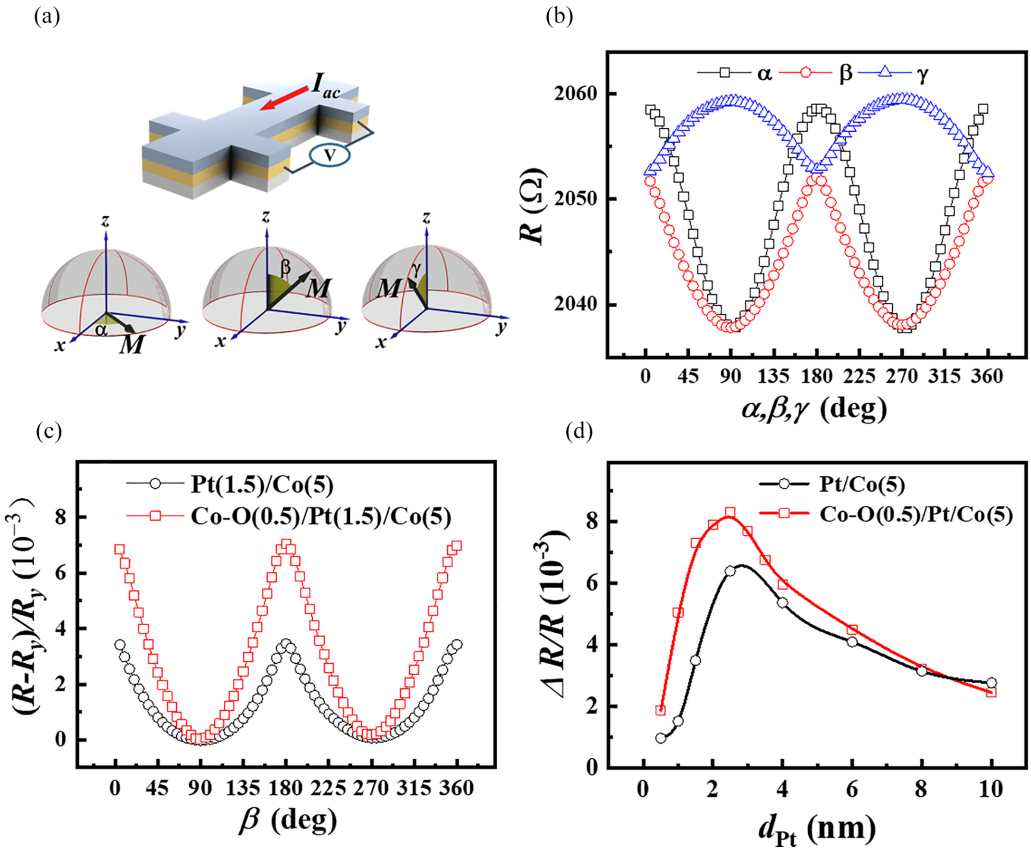

FIG. 5. Spin Hall magnetoresistance (SMR) measurements for the Co-O(0.5)/Pt/Co(5) and control samples. (a) The schematic diagram of the longitudinal resistance measurement setup and the definition of the coordinate system. (b) Angular dependences of longitudinal resistance in three orthogonal planes for the Co-O(0.5)/Pt(1.5)/Co(5) sample. (c) The normalized resistance variation in the yz plane for the Co-O(0.5)/Pt(1.5)/Co(5) sample and its comparison with the control sample [Pt(1.5)/Co(5)]. (d) Pt thickness dependence of the SMR ratio for the Co-O(0.5)/Pt(t_{Pt})/Co(5) samples and its comparison with the control sample [Pt(t_{Pt})/Co(5)].

reflected by the FM layer depending on the relative orientation of the spin polarization and the magnetization direction of the FM layer. The reflected spin current may transform back to a charge current in the HM layer via the inverse SHE, resulting in the resistance difference with respect to the magnetization orientation of the magnetic layer. Supposing that an additional angular momentum accumulation is produced in this structure due to the OREE effect at the Co-O/Pt interface, which may transform to spin current due to the large SOC in the Pt layer, then we expect that the extra spin current may also result in the enhancement of SMR. We performed the angular-dependent MR (ADMR) measurement for group-B samples by rotating the applied field of $H = 15$ kOe in the yz plane (β), xz plane (γ), and xy plane (α), as shown in Fig. 5(a). Figure 5(b) shows the typical angular dependence of R in different planes for the Co-O(0.5)/Pt(1.5)/Co(5) sample. We noted that the Co-O underlayer does not affect the MR in the xz plane remarkably, but it enhances the MR in the yz and xy planes. Here, we focus on the MR in the yz plane scan because it is closely related to the pure SMR effect. Figure 5(c) shows the ADMR measurement results in the yz plane for the Co-O/Pt(1.5)/Co samples and its comparison with the control sample (without the Co-O underlayer). We noted that the SMR ratio (defined as $\Delta R/R = (R_z - R_y)/R_y$, where R_y (R_z) is the measured longitudinal resistance when the magnetization is saturated parallel to the y (z) direction, for the Co-O(0.5)/Pt(1.5)/Co(5) sample is almost twice that of the Pt(1.5)/Co(5) control sample. The SMR ratios for the samples with different t_{Pt}'s were summarized in Fig. 5(d). The significant enhancement of SMR is observed when t_{Pt} is small, and the enhancement disappears gradually as t_{Pt} becomes large. In combination with the previous discussion, we believe that the enhancement of SMR in the Co-O/Pt/Co samples originates from the spin current converted from the orbital current, and the effect degrades certainly as the Pt layer thickness exceeds its spin-diffusion length.

Finally, we verify the extra SOT from the Co-O/Pt interface by the loop-shift method [59] and the current-induced magnetization switching in the group-C samples. To obtain PMA, the as-deposited Co layers were set to 1.8 nm in the Pt/Co/Co-O/Pt sample and 1.0 nm in the Pt/Co/Pt control samples. Therefore, after natural oxidation, the Co layers have the same thickness (1.0 nm) in all the samples, and they exhibit strong PMA. The SOT is quantitatively estimated by using the hysteresis loop-shift technique, as shown in Fig. 6(a). We measured the Hall resistance R_H vs the out-of-plane field (H_z) in the Hall-bar devices with different current magnitude and in-plane bias field H_x. Figure 6(b) shows the representative R_H-H_z loops for the Pt(3)/Co/Co-O/Pt (3) sample with $I = \pm 8$ mA and $H_x = 4$ kOe. The significant loop shift (ΔH)

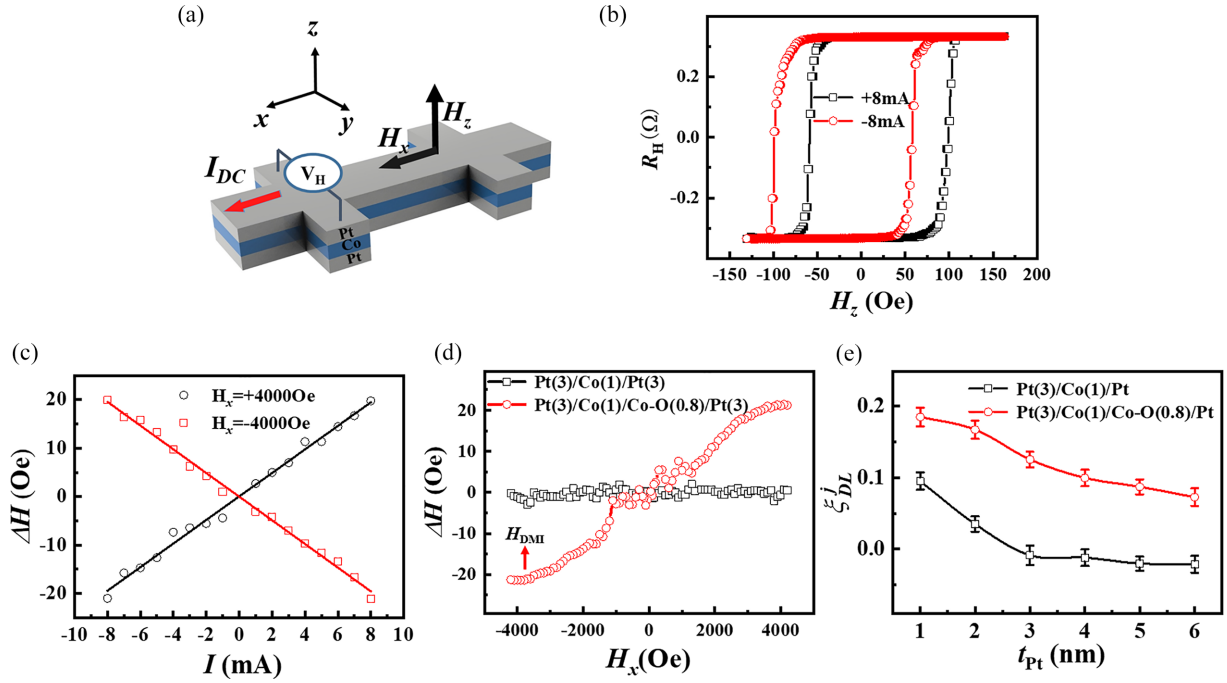

FIG. 6. Dampinglike spin-orbit torque (DL-SOT) effective field measurement for the Pt/Co/(Co-O)/Pt structure by the loop-shift method. (a) The schematic diagram of the measurement method; (b) the representative R_H-H_Z loops under $I = \pm 8$ mA and $H_x = 4$ kOe for the Pt(3)/Co/Co-O/Pt(3) sample; and (c) the measured ΔH with different I's and the linear fitting to the ΔH-I curves at $H_x = \pm 4$ kOe. (d) Variation of ΔH as a function of H_x and its comparison with the control sample (without the Co-O layer). (e)The calculated DL-SOT efficiency for the samples with different t_{Pt}'s.

suggests the presence of a net out-of-plane effective field in the sample, which is unobservable in the Pt(3)/Co/Pt(3) control sample since the spin currents from both Pt layers cancel out. Figure 6(c) summarizes the obtained ΔH values as a function of current magnitude with $H_x = \pm 4$ kOe. It is noted that ΔH scales linearly with current magnitude, and its sign depends on the bias field direction. Further, ΔH values at different H_x's are summarized in Fig. 6(d), which increases with H_x and saturates when H_x is equal to the Dzyaloshinskii-Moriya interaction (DMI) effective field (H_{DMI}). The saturation value of the ΔH-H_x curve corresponds to the effective DL field, from which we can obtain the SOT efficiency per unit current density for the samples with different top Pt layer thickness, as shown in Fig. 6(e). The large discrepancy between the DL-SOT efficiencies in the Pt/Co/Pt and Pt/Co/Co-O/Pt samples implies the additional SOT origin in the oxidized samples. Although the depression to the spin current from the top Pt layer by the interface oxide layer can also qualitatively explain this behavior, it will lead to a completely different dependence of SOT efficiency on the thickness of the upper Pt layer.

The SOT-driven magnetization switching is also demonstrated in the Pt/Co/Pt and Pt/Co/Co-O/Pt samples. In this experiment, a constant in-plane field (H_x) was applied along the current channel of the Hall-bar devices, and the current pulses with pulse width of 0.5 ms were injected into the

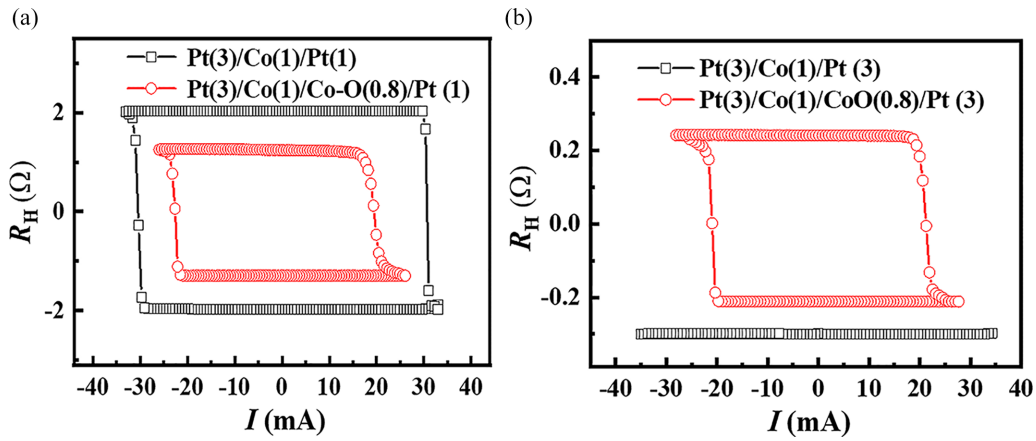

FIG. 7. Current-induced magnetization switching curves for the Pt(3)/Co(1.0)/Pt(t_{Pt}) and Pt(3)/Co(1)/Co-O(0.8)/Pt(t_{Pt}) structures with (a) $t_{Pt} = 1$ nm and (b) $t_{Pt} = 3$ nm under $H_x = 1$ kOe.

devices with ascending or descending magnitude. The constant H_x can break the symmetry along the current direction and helps to achieve SOT-induced magnetization switching. The magnetization state of the Co layer was monitored by the anomalous Hall voltage measured in the interval between the pulses with a small current of 1 mA. Figure 7 shows the current-induced magnetization switching curves for the Pt(3)/Co(1.0)/Pt(t_{Pt}) and Pt(3)/Co(1)/Co-O(0.8)/Pt(t_{Pt}) structures with $t_{Pt} = 1$ nm (a) and $t_{Pt} = 3$ nm (b) under $H_x = 1$ kOe. The complete switching loops are observed for both Pt(3)/Co(1)/Pt(1) and Pt(3)/Co(1)/Co-O(0.8)/Pt(1) samples. The critical switching current for the oxidized sample is significantly smaller than the unoxidized sample, indicating the enhanced SOT in the former. In addition, the current-induced magnetization switching was also observed in the Pt(3)/Co(1)/Co-O(0.8)/Pt(3) sample, while for the Pt(3)/Co(1)/Pt(3) sample with symmetrical structure, no switching behavior was observed, even when the current pulse with larger magnitude was applied. Although the critical switching current depends on many factors, it can also reflect the SOT efficiency of the system.

In summary, from the SOT, SMR, and current-induced magnetization switching measurement results in three groups of samples, we found a new SOT origin at the Co-O/Pt interface. The significant FM thickness dependence of the extra SOT in the Co/Co-O/Pt structures fit with the fingerprint of the orbital current-induced torques. Considering the weak SOC of Co-O, we attribute the anomalous SOT and SMR manipulation in the samples to the OREE at the Co-O/Pt interface. Our findings not only provide a strategy for generating additional spin currents to manipulate the SOT but also demonstrate an important clue toward a microscopic understanding of how the out-of-equilibrium OAM interacts with the local magnetization.

The data that support the findings of this study are available from the corresponding author upon reasonable request.

This paper was supported by the National Natural Science Foundation of China (NNSFC) (Grants No. 51771099 and No. 11674142) and the Science and Technology Program of Gansu Province (Grant No. 20JR5RA266).

[1] L. Liu, O. J. Lee, T. J. Gudmundsen, D. C. Ralph, and R. A. Buhrman, Current-induced switching of perpendicularly magnetized magnetic layers using spin torque from the spin Hall effect, Phys. Rev. Lett. **109**, 096602 (2012).

[2] L. Liu, T. Moriyama, D. C. Ralph, and R. A. Buhrman, Spin-torque ferromagnetic resonance induced by the spin Hall effect, Phys. Rev. Lett. **106**, 036601 (2011).

[3] A. Manchon, J. Zelezny, I. M. Miron, T. Jungwirth, J. Sinova, A. Thiaville, K. Garello, and P. Gambardella, Current-induced spin-orbit torques in ferromagnetic and antiferromagnetic systems, Rev. Mod. Phys. **91**, 035004 (2019).

[4] A. Brataas, A. D. Kent, and H. Ohno, Current-induced torques in magnetic materials, Nat. Mater. **11**, 372 (2012).

[5] H. An, Y. Kageyama, Y. Kanno, N. Enishi, and K. Ando, Spin-torque generator engineered by natural oxidation of Cu, Nat. Commun. **7**, 13069 (2016).

[6] C.-F. Pai, Y. Ou, L. H. Vilela-Leão, D. C. Ralph, and R. A. Buhrman, Dependence of the efficiency of spin Hall torque on the transparency of Pt/ferromagnetic layer interfaces, Phys. Rev. B **92**, 064426 (2015).

[7] M. E. Stebliy, A. G. Kolesnikov, A. V. Ognev, A. V. Davydenko, E. V. Stebliy, X. Wang, X. Han, and A. S. Samardak, Advanced method for the reliable estimation of spin-orbit-torque efficiency in low-coercivity ferromagnetic multilayers, Phys. Rev. Appl. **11**, 054047 (2019).

[8] L. Zhu and R. A. Buhrman, Maximizing spin-orbit-torque efficiency of Pt/Ti multilayers: Trade-off between intrinsic spin Hall conductivity and carrier lifetime, Phys. Rev. Appl. **12**, 051002(R) (2019).

[9] J. E. Hirsch, Spin Hall effect, Phys. Rev. Lett. **83**, 1834 (1999).

[10] J. Sinova, S. O. Valenzuela, J. Wunderlich, C. H. Back, and T. Jungwirth, Spin Hall effects, Rev. Mod. Phys. **87**, 1213 (2015).

[11] A. Hoffmann, Spin Hall effects in metals, IEEE Trans. Magn. **49**, 5172 (2013).

[12] O. Krupin, G. Bihlmayer, K. Starke, S. Gorovikov, J. E. Prieto, K. Döbrich, S. Blügel, and G. Kaindl, Rashba effect at magnetic metal surfaces, Phys. Rev. B **71**, 201403(R) (2005).

[13] J. C. Sanchez, L. Vila, G. Desfonds, S. Gambarelli, J. P. Attane, J. M. De Teresa, C. Magen, and A. Fert, Spin-to-charge conversion using Rashba coupling at the interface between non-magnetic materials, Nat. Commun. **4**, 2944 (2013).

[14] G. Y. Guo, S. Murakami, T. W. Chen, and N. Nagaosa, Intrinsic spin Hall effect in platinum: First-principles calculations, Phys. Rev. Lett. **100**, 096401 (2008).

[15] M. H. Nguyen, D. C. Ralph, and R. A. Buhrman, Spin torque study of the spin Hall conductivity and spin diffusion length in platinum thin films with varying resistivity, Phys. Rev. Lett. **116**, 126601 (2016).

[16] L. Zhu, D. C. Ralph, and R. A. Buhrman, Maximizing spin-orbit torque generated by the spin Hall effect of Pt, Appl. Phys. Rev. **8**, 031308 (2021).

[17] L. Zhu, L. Zhu, S. Shi, M. Sui, D. C. Ralph, and R. A. Buhrman, Enhancing spin-orbit torque by strong interfacial scattering from ultrathin insertion layers, Phys. Rev. Appl. **11**, 061004(R) (2019).

[18] L. Zhu, D. C. Ralph, and R. A. Buhrman, Highly efficient spin-current generation by the spin Hall effect in $Au_{1-x}Pt_x$, Phys. Rev. Appl. **10**, 031001(R) (2018).

[19] L. Zhu, K. Sobotkiewich, X. Ma, X. Li, D. C. Ralph, and R. A. Buhrman, Strong damping-like spin-orbit torque and tunable Dzyaloshinskii-Moriya interaction generated by low-resistivity $Pd_{1-x}Pt_x$ alloys, Adv. Funct. Mater. **29**, 1805822 (2019).

[20] D. Go and H.-W. Lee, Orbital torque: Torque generation by orbital current injection, Phys. Rev. Res. **2**, 013177 (2020).

[21] D. Go, D. Jo, C. Kim, and H.-W. Lee, Intrinsic spin and orbital Hall effects from orbital texture, Phys. Rev. Lett. **121**, 086602 (2018).

[22] D. Jo, D. Go, and H.-W. Lee, Gigantic intrinsic orbital Hall effects in weakly spin-orbit coupled metals, Phys. Rev. B **98**, 214405 (2018).
[23] G. Sala and P. Gambardella, Giant orbital Hall effect and orbital-to-spin conversion in $3d$, $5d$, and $4f$ metallic heterostructures, Phys. Rev. Res. **4**, 033037 (2022).
[24] Y.-G. Choi, D. Jo, K.-H. Ko, D. Go, K.-H. Kim, H. G. Park, C. Kim, B.-C. Min, G.-M. Choi, and H.-W. Lee, Observation of the orbital Hall effect in a light metal Ti, Nature (London) **619**, 52 (2023).
[25] D. Go, J.-P. Hanke, P. M. Buhl, F. Freimuth, G. Bihlmayer, H.-W. Lee, Y. Mokrousov, and S. Blügel, Toward surface orbitronics: Giant orbital magnetism from the orbital Rashba effect at the surface of *sp*-metals, Sci. Rep. **7**, 46742 (2017).
[26] X. Chen, Y. Liu, G. Yang, H. Shi, C. Hu, M. Li, and H. Zeng, Giant antidamping orbital torque originating from the orbital Rashba-Edelstein effect in ferromagnetic heterostructures, Nat. Commun. **9**, 2569 (2018).
[27] L. Salemi, M. Berritta, A. K. Nandy, and P. M. Oppeneer, Orbitally dominated Rashba-Edelstein effect in noncentrosymmetric antiferromagnets, Nat. Commun. **10**, 5381 (2019).
[28] D. Go, D. Jo, T. Gao, K. Ando, S. Blügel, H.-W. Lee, and Y. Mokrousov, Orbital Rashba effect in a surface-oxidized Cu film, Phys. Rev. B **103**, L121113 (2021).
[29] S. Ding, A. Ross, D. Go, L. Baldrati, Z. Ren, F. Freimuth, S. Becker, F. Kammerbauer, J. Yang, G. Jakob *et al.*, Harnessing orbital-to-spin conversion of interfacial orbital currents for efficient spin-orbit torques, Phys. Rev. Lett. **125**, 177201 (2020).
[30] S. Bhowal and G. Vignale, Orbital Hall effect as an alternative to valley Hall effect in gapped graphene, Phys. Rev. B **103**, 195309 (2021).
[31] M. Ünzelmann, H. Bentmann, P. Eck, T. Kißlinger, B. Geldiyev, J. Rieger, S. Moser, R. C. Vidal, K. Kißner, L. Hammer *et al.*, Orbital-driven Rashba effect in a binary honeycomb monolayer AgTe, Phys. Rev. Lett. **124**, 176401 (2020).
[32] J. Kim, D. Go, H. Tsai, D. Jo, K. Kondou, H.-W. Lee, and Y. C. Otani, Nontrivial torque generation by orbital angular momentum injection in ferromagnetic-metal/Cu/Al_2O_3 trilayers, Phys. Rev. B **103**, L020407 (2021).
[33] J. Kim, J. Uzuhashi, M. Horio, T. Senoo, D. Go, D. Jo, T. Sumi, T. Wada, I. Matsuda, T. Ohkubo *et al.*, Oxide layer dependent orbital torque efficiency in ferromagnet/Cu/oxide heterostructures, Phys. Rev. Mater. **7**, L111401 (2023).
[34] S. Krishnia, B. Bony, E. Rongione, L. M. Vicente-Arche, T. Denneulin, A. Pezo, Y. Lu, R. E. Dunin-Borkowski, S. Collin, A. Fert *et al.*, Quantifying the large contribution from orbital Rashba-Edelstein effect to the effective damping-like torque on magnetization, APL. Mater. **12**, 051105 (2024).
[35] T.-Y. Chen, Y.-C. Hsiao, W.-B. Liao, and C.-F. Pai, Tailoring neuromorphic switching by CuN_x-mediated orbital currents, Phys. Rev. Appl. **17**, 064005 (2022).
[36] E. Santos, J. E. Abrão, D. Go, L. K. de Assis, Y. Mokrousov, J. B. S. Mendes, and A. Azevedo, Inverse orbital torque via spin-orbital intertwined states, Phys. Rev. Appl. **19**, 014069 (2023).
[37] S. Ding, Z. Liang, D. Go, C. Yun, M. Xue, Z. Liu, S. Becker, W. Yang, H. Du, C. Wang *et al.*, Observation of the orbital Rashba-Edelstein magnetoresistance, Phys. Rev. Lett. **128**, 067201 (2022).
[38] S. Ding, P. Noël, G. K. Krishnaswamy, and P. Gambardella, Unidirectional orbital magnetoresistance in light-metal-ferromagnet bilayers, Phys. Rev. Res. **4**, L032041 (2022).
[39] X. Qiu, K. Narayanapillai, Y. Wu, P. Deorani, D. H. Yang, W. S. Noh, J. H. Park, K. J. Lee, H. W. Lee, and H. Yang, Spin-orbit-torque engineering via oxygen manipulation, Nat. Nanotechnol. **10**, 333 (2015).
[40] Y. Hibino, T. Hirai, K. Hasegawa, T. Koyama, and D. Chiba, Enhancement of the spin-orbit torque in a Pt/Co system with a naturally oxidized Co layer, Appl. Phys. Lett. **111**, 132404 (2017).
[41] K. Hasegawa, Y. Hibino, M. Suzuki, T. Koyama, and D. Chiba, Enhancement of spin-orbit torque by inserting CoO_x layer into Co/Pt interface, Phys. Rev. B **98**, 020405(R) (2018).
[42] S. Haku, A. Musha, T. Gao, and K. Ando, Role of interfacial oxidation in the generation of spin-orbit torques, Phys. Rev. B **102**, 024405 (2020).
[43] Z. Liao and J. Zhang, Metal-to-insulator transition in ultrathin manganite heterostructures, Appl. Sci. **9**, 144. (2019).
[44] H. Chen, Y. Yu, Z. Wang, Y. Bai, H. Lin, X. Li, H. Liu, T. Miao, Y. Kou, Y. Zhang *et al.*, Thickness-driven first-order phase transitions in manganite ultrathin films, Phys. Rev. B **99**, 214419 (2019).
[45] See Supplemental Material at http://link.aps.org/supplemental/10.1103/PhysRevB.110.104404 for detailed information on determination of the Co-O layer thickness and saturation magnetization of Co, the exclusion of the SOT contribution from the bulk Co-O and the Co/Co-O interface in the Co/Co-O/Pt samples, the temperature dependence of SOT for a typical Co(4.2)/Co-O(0.8)/Pt(5) sample, and the discussion on the spin and the OAM direction in these structures.
[46] C. O. Avci, K. Garello, M. Gabureac, A. Ghosh, A. Fuhrer, S. F. Alvarado, and P. Gambardella, Interplay of spin-orbit torque and thermoelectric effects in ferromagnet/normal-metal bilayers, Phys. Rev. B **90**, 224427 (2014).
[47] M. Hayashi, J. Kim, M. Yamanouchi, and H. Ohno, Quantitative characterization of the spin-orbit torque using harmonic Hall voltage measurements, Phys. Rev. B **89**, 144425 (2014).
[48] X. Qiu, W. Legrand, P. He, Y. Wu, J. Yu, R. Ramaswamy, A. Manchon, and H. Yang, Enhanced spin-orbit torque via modulation of spin current absorption, Phys. Rev. Lett. **117**, 217206 (2016).
[49] Y. Lim, S. Wu, D. A. Smith, C. Klewe, P. Shafer, and S. Emori, Absorption of transverse spin current in ferromagnetic NiCu: Dominance of bulk dephasing over spin-flip scattering, Appl. Phys. Lett. **121**, 222403 (2022).
[50] Q. Li, M. Yang, C. Klewe, P. Shafer, A. T. N'Diaye, D. Hou, T. Y. Wang, N. Gao, E. Saitoh, C. Hwang *et al.*, Coherent ac spin current transmission across an antiferromagnetic CoO insulator, Nat. Commun. **10**, 5265 (2019).
[51] T. Ikebuchi, T. Moriyama, H. Mizuno, K. Oda, and T. Ono, Spin current transmission in polycrystalline NiO films, Appl. Phys. Express **11**, 073003 (2018).
[52] D. Hou, Z. Qiu, J. Barker, K. Sato, K. Yamamoto, S. Vélez, J. M. Gomez-Perez, L. E. Hueso, F. Casanova, and E. Saitoh, Tunable sign change of spin Hall magnetoresistance in Pt/NiO/YIG structures, Phys. Rev. Lett. **118**, 147202 (2017).
[53] S. Okamoto, Spin injection and spin transport in paramagnetic insulators, Phys. Rev. B **93**, 064421 (2016).

[54] K. Oyanagi, S. Takahashi, L. J. Cornelissen, J. Shan, S. Daimon, T. Kikkawa, G. E. W. Bauer, B. J. van Wees, and E. Saitoh, Spin transport in insulators without exchange stiffness, Nat. Commun. **10**, 4740 (2019).

[55] H. Hayashi, D. Jo, D. Go, T. Gao, S. Haku, Y. Mokrousov, H.-W. Lee, and K. Ando, Observation of long-range orbital transport and giant orbital torque, Commun. Phys. **6**, 32 (2023).

[56] Y.-T. Chen, S. Takahashi, H. Nakayama, M. Althammer, S. T. B. Goennenwein, E. Saitoh, and G. E. W. Bauer, Theory of spin Hall magnetoresistance, Phys. Rev. B **87**, 144411 (2013).

[57] J. Kim, P. Sheng, S. Takahashi, S. Mitani, and M. Hayashi, Spin Hall magnetoresistance in metallic bilayers, Phys. Rev. Lett. **116**, 097201 (2016).

[58] H. Nakayama, Y. Kanno, H. An, T. Tashiro, S. Haku, A. Nomura, and K. Ando, Rashba-Edelstein magnetoresistance in metallic heterostructures, Phys. Rev. Lett. **117**, 116602 (2016).

[59] C.-F. Pai, M. Mann, A. J. Tan, and G. S. D. Beach, Determination of spin torque efficiencies in heterostructures with perpendicular magnetic anisotropy, Phys. Rev. B **93**, 144409 (2016).